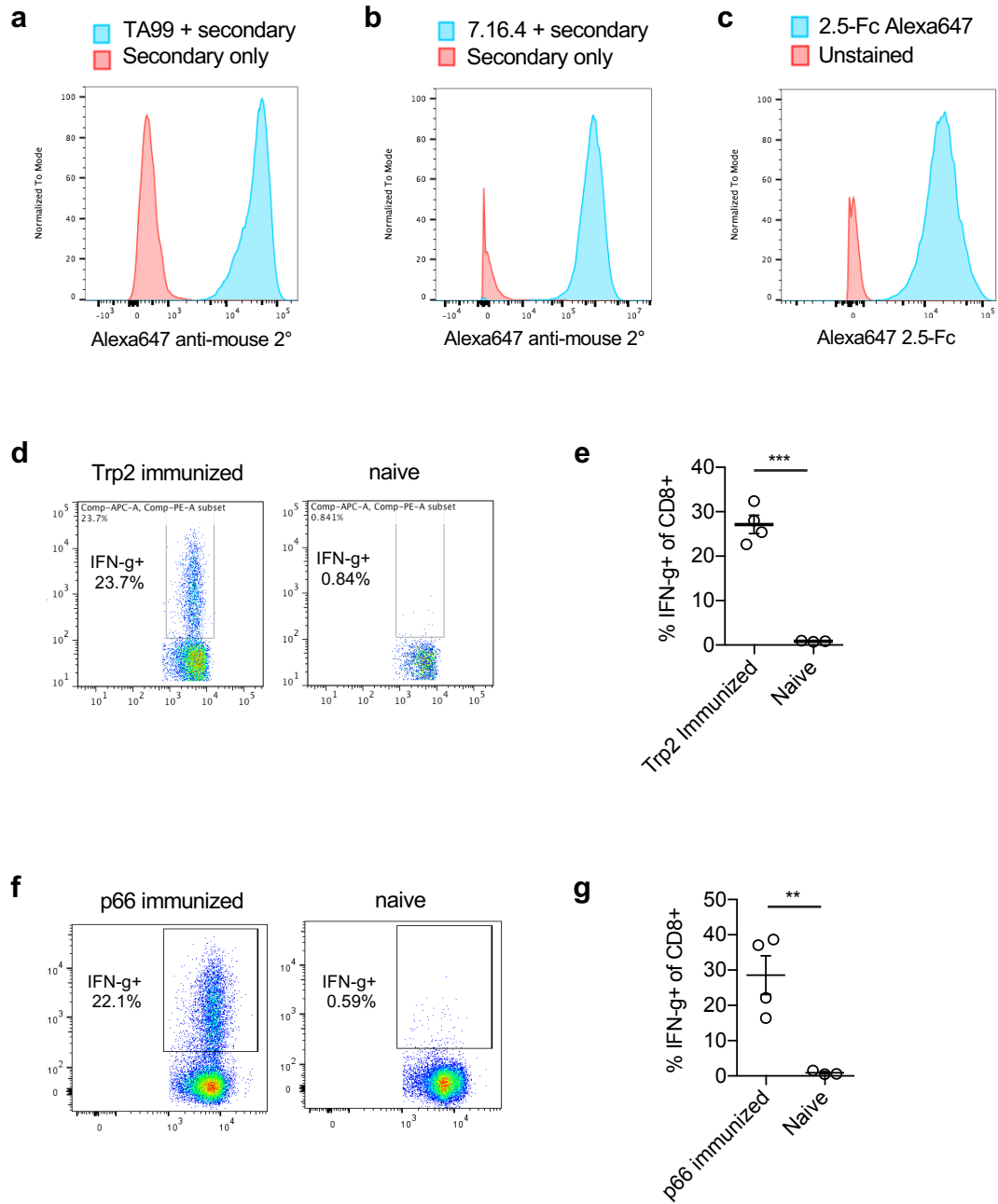
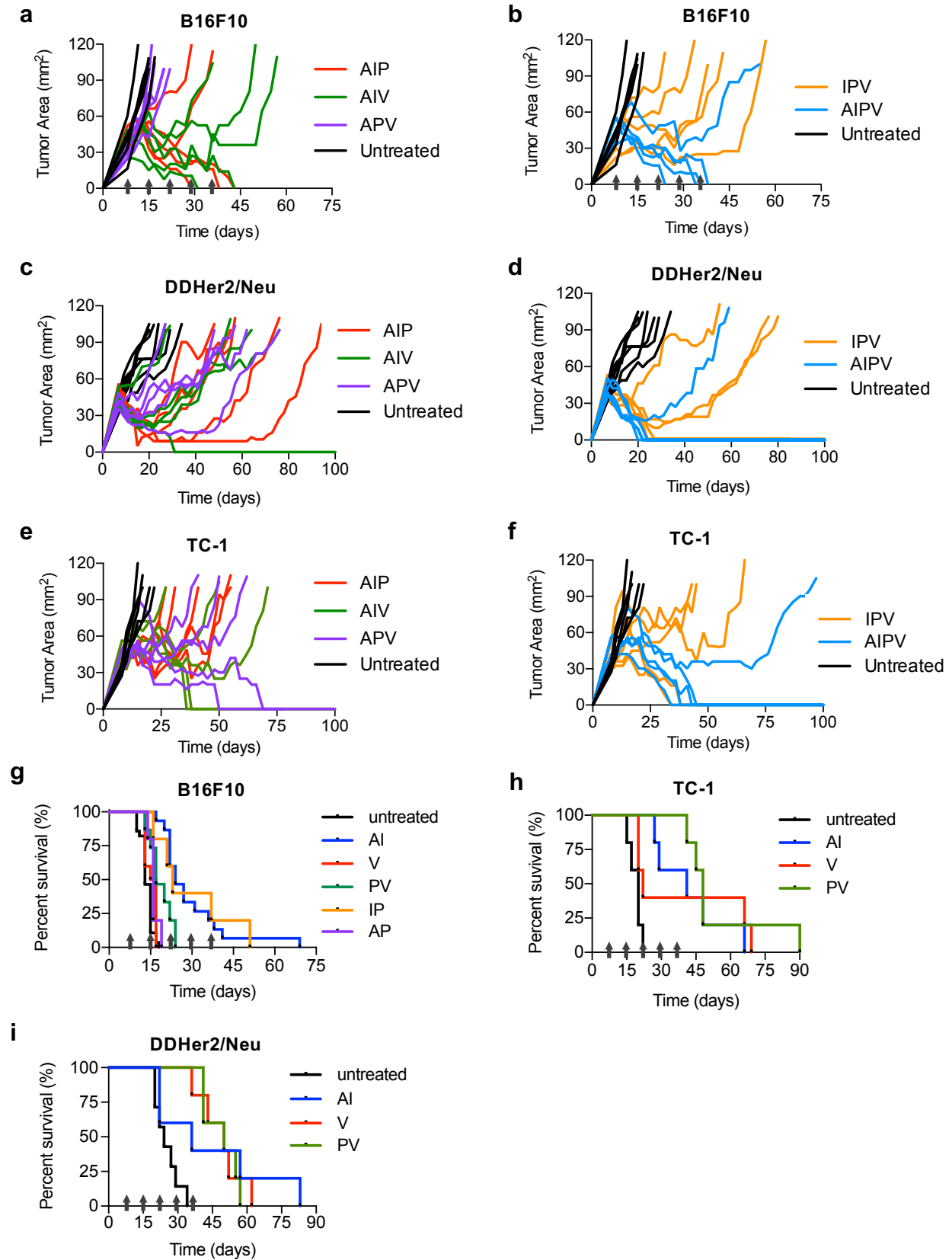


# Supplementary Fig. 1



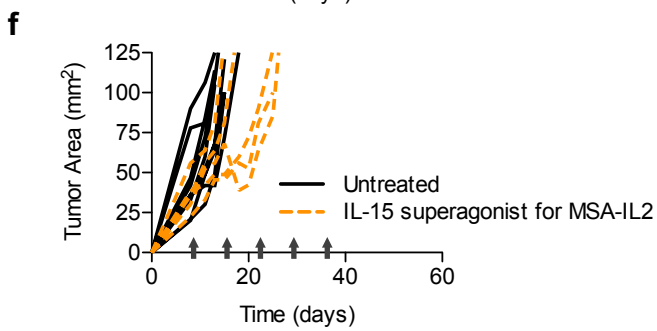
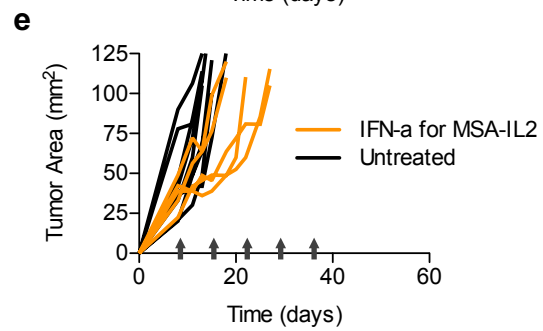
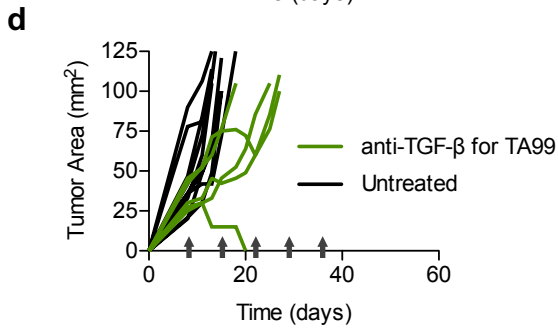
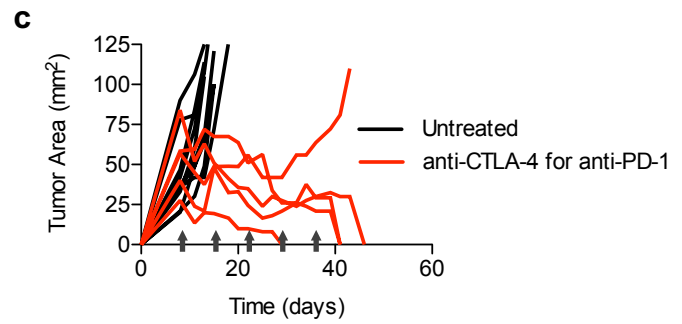
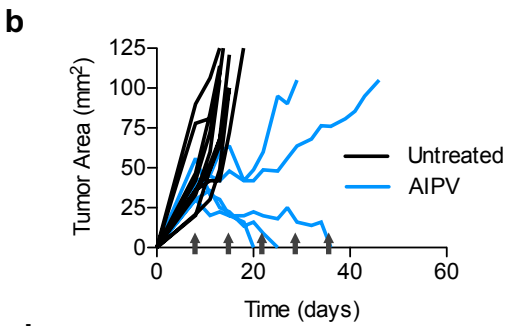
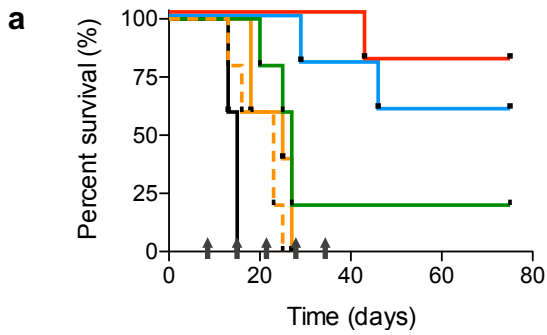
**Supplementary Figure 1: Selection of A (monoclonal anti-tumor antibody) and V (amphiphile-vaccine) components for treatment of B16F10, DD-Her2/Neu, and TC-1 tumors.** **a**, B16F10 cells were incubated with 20 $\mu$ g/mL TA99 for 20 minutes at 4°C, washed, and stained with AlexaFluor647 labeled anti-mouse IgG followed by flow cytometry analysis. **b**, DD-Her2/neu cells were incubated with 20 $\mu$ g/mL 7.16.4 for 20 minutes at 4°C, washed, and stained with AlexaFluor647 labeled anti-mouse IgG followed by flow cytometry. **c**, TC-1 cells were incubated with 20 $\mu$ g/mL AlexaFluor647 labeled 2.5-Fc for 20 minutes at 4°C, washed, and analyzed by flow cytometry. **d-e**, C57Bl/6 mice ( $n = 4$  animals/group) were primed and boosted 14 days later with amph-vaccine (20  $\mu$ g amph-Trp2 and 1.24 nmol amph-CpG) against Trp-2. Six days following the boost, intracellular cytokine staining was performed on peripheral blood cells to quantify anti-Trp2 responses. Shown are representative plots (**d**) and mean $\pm$ s.e.m. %IFN- $\gamma^+$  among CD8 $^+$  T-cells (**e**). **f-g**, Balb/c mice ( $n = 4$  animals/group) were primed and boosted 14 days later with amph-vaccine against p66 (20  $\mu$ g amph-p66 and 1.24 nmol amph-CpG). Six days following boost, ICS was performed to quantify anti-p66 responses. Shown are representative plots (**e**) and mean $\pm$ s.e.m. %IFN- $\gamma$  among CD8 $^+$  T-cells (**f**).

# Supplementary Fig. 2



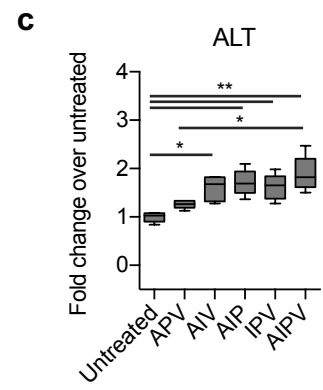
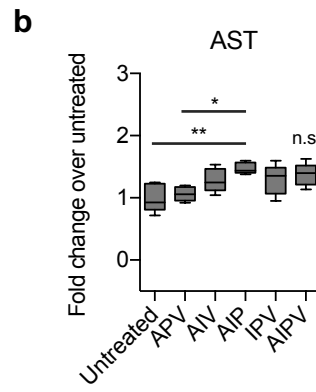
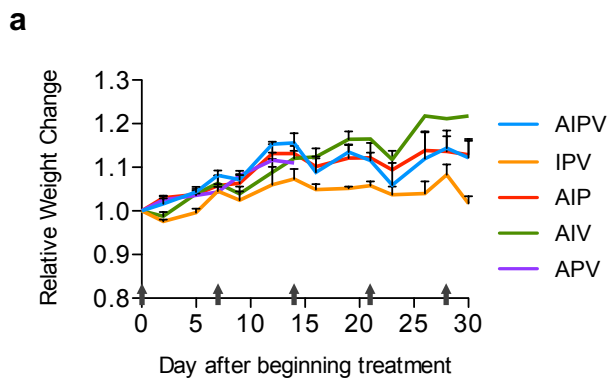
**Supplementary Figure 2: Individual tumor growth kinetics and therapeutic efficacy of single and double agent therapies in B16F10, DD-Her2/Neu, and TC-1 tumor models. a-h,** Groups of mice were inoculated with  $10^6$  tumor cells s.c. in the flank: B16F10 (**a-b**,  $n = 5$  animals/group, representative of 4 independent experiments, **c-d**,  $n = 5$ /group for untreated and IP, 20 animals/group V, PV, and AI) and TC-1 (**g-h**,  $n = 5$  animals/group) tumor cells were injected in C57Bl/6 mice while DD-Her2/neu tumor cells (**e-f**,  $n = 5$  animals/group) were injected in balb/c mice. On day 8 post implantation, treatment was initiated following the timeline in Fig. 1a using the indicated paired or individual components of AIPV. Shown are individual mice (**a, b**), or mean tumor area  $\pm$  s.e.m (**c, e, g**) and survival. Arrows indicate treatment time points.

# Supplementary Fig. 3



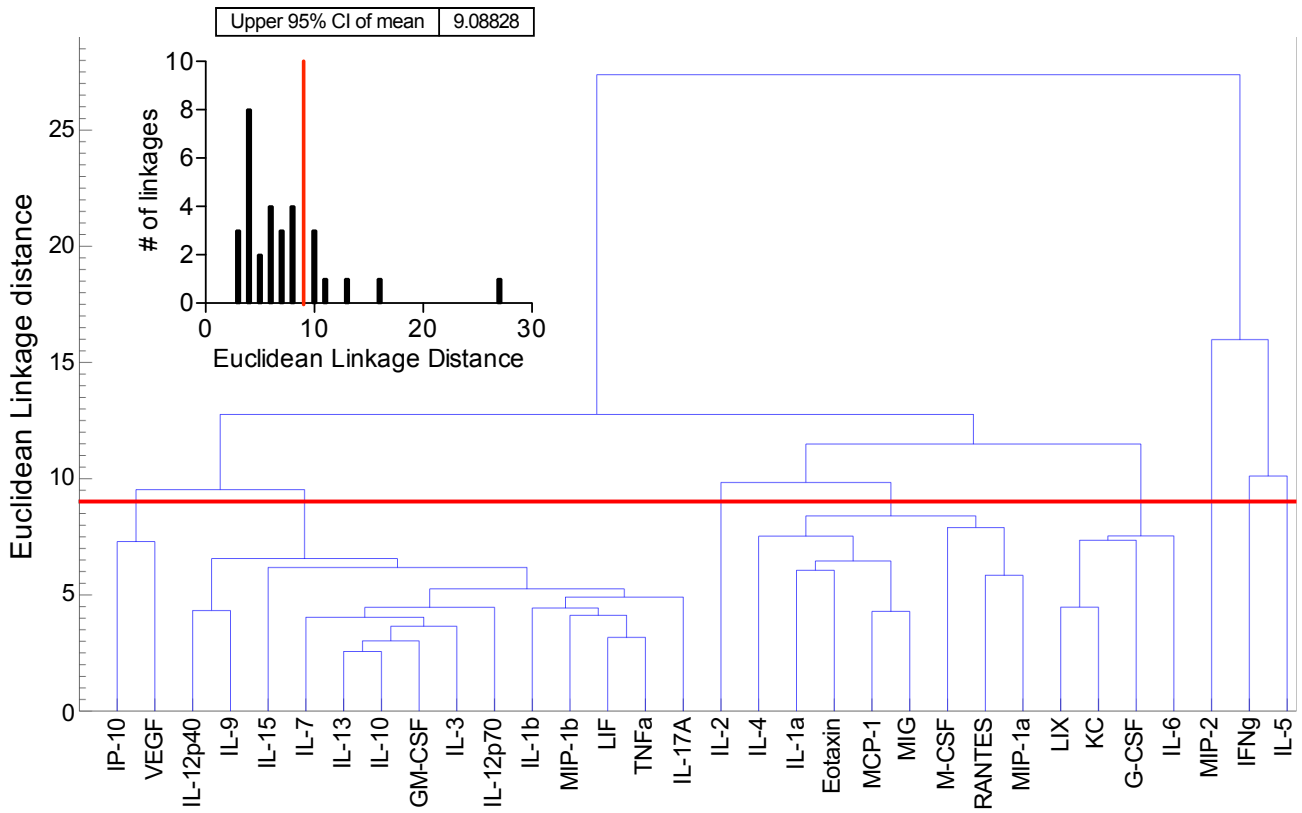
**Supplementary Figure 3: Exploration of alternative quaternary combination therapies for treatment of B16F10 melanomas.** Groups of C57Bl/6 mice ( $n = 5$  animals/group) were inoculated with  $10^6$  B16F10 cells s.c. in the flank. On day 8 post implantation, treatment was initiated following the timeline in Fig. 1a with either AIPV or with quaternary treatments substituting one of the components of AIPV with an alternative immunotherapy agent as indicated (see Methods). Shown are survival (**a**) and tumor growth in individual mice (**b-g**). Shown are survival (**a**), and mean tumor area  $\pm$  s.e.m (**b-f**). Arrows indicate treatment time points. \*  $P < 0.05$ , \*\*  $P < 0.01$ , \*\*\*  $P < 0.001$  versus AIPV by Log-rank (Mantel-Cox) test.

# Supplementary Fig. 4



**Supplementary Figure 4: AIPV therapy is well tolerated but accompanied by pronounced vitiligo.** **a-c**, C57Bl/6 mice ( $n = 5$  animals/group) were inoculated with  $10^6$  B16F10 cells s.c. in the flank and treatment was initiated following the timeline in Fig. 1a. Shown are body weight measurements over time normalized to initial weights (**a**) and analysis of serum AST and ALT liver enzyme levels in serum of mice 36 hours after treatment initiation (**b-c**, whiskers are 5-95%). **d-e**, representative images of AIPV treated mice 65 days (**d**) and 125 days (**e**) after tumor inoculation. **f**, non-tumor bearing mice were primed and boosted 14 days later with amph-Trp2 vaccine. Shown are representative images at 111 days after boost; no vitiligo was detected. Images in **d-f** are representative of 2-5 independent experiments. Arrows indicate treatment time points.  $*P < 0.05$ ,  $**P < 0.01$ ,  $***P < 0.001$  by one-way ANOVA with Bonferroni post-test, n.s. not significant for all comparisons.

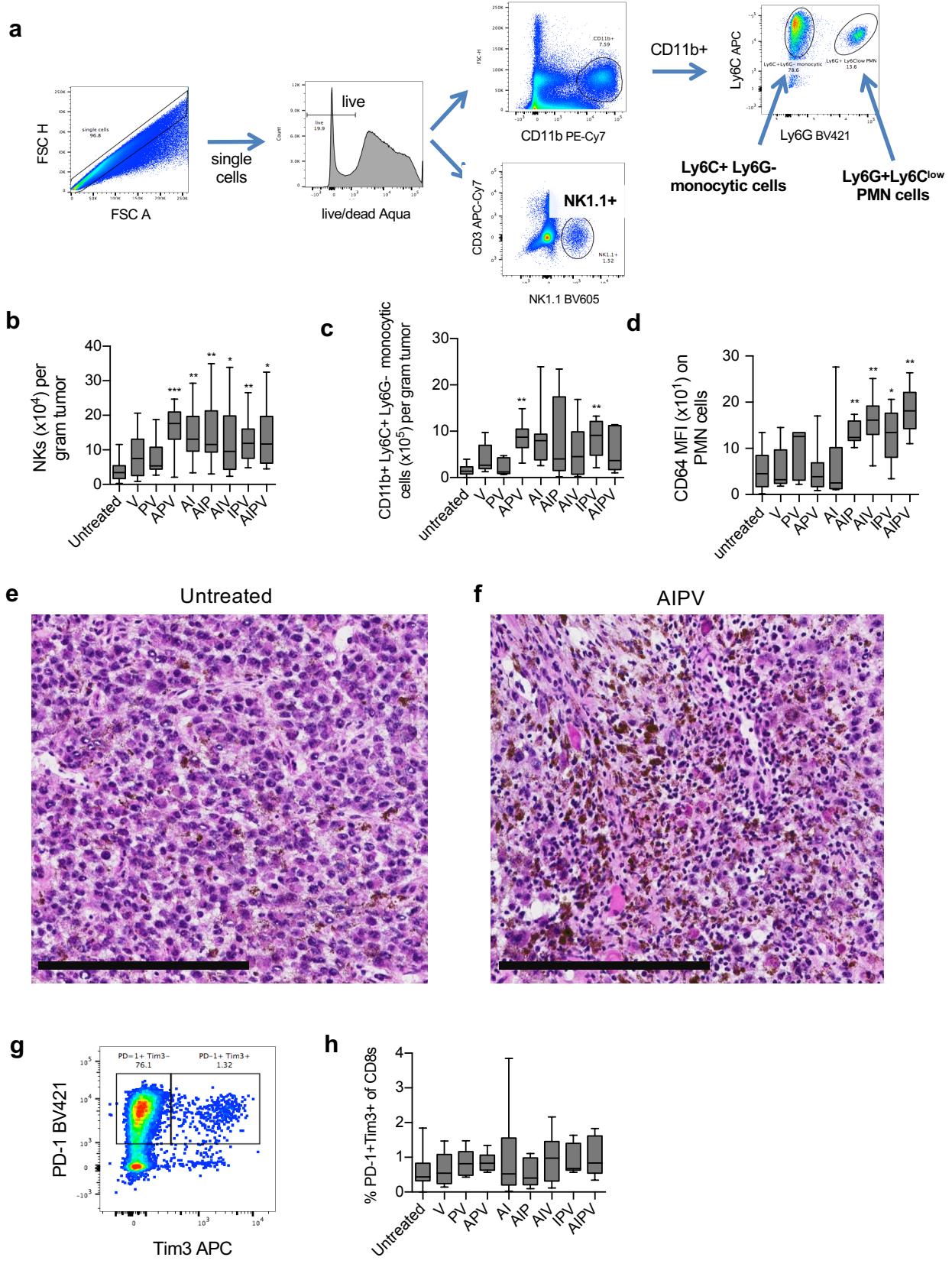
# Supplementary Fig. 5



**Supplementary Figure 5: Extended analysis of intratumoral cytokines/chemokine profiles.**

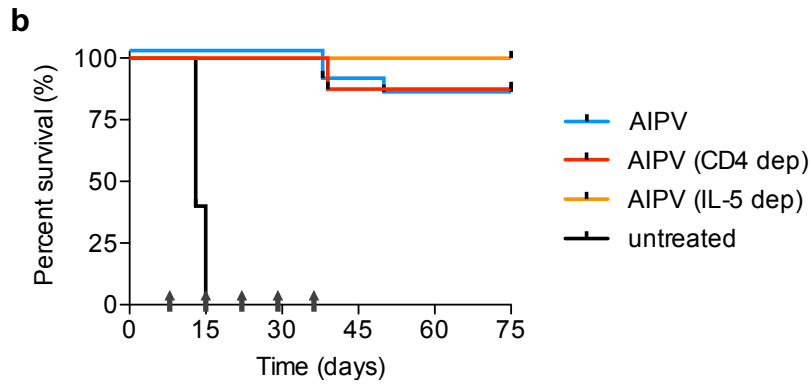
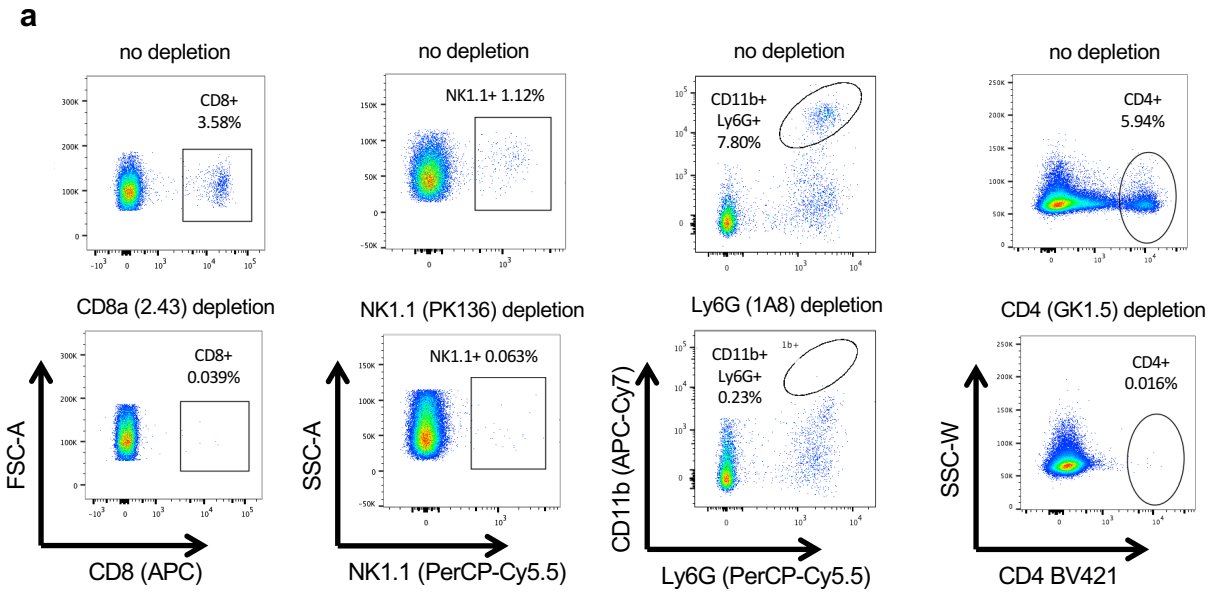
C57Bl/6 mice were inoculated with  $10^6$  B16F10 cells s.c. in the flank and treatment with AIPV or subcombination therapies was initiated following the timeline in Fig. 1a. Tumors were analyzed on day 17. A hierarchical binary cluster tree was created using Euclidean Linkage distance for log<sub>2</sub>-fold change of all cytokines and chemokines measured; each protein was designated a leaf. Tree pruning was performed by collapsing all leaves with a linkage distance less than the 95% confidence interval (red line).

# Supplementary Fig. 6



**Supplementary Figure 6: Immune cell infiltration during AIPV therapy.** C57Bl/6 mice were inoculated with  $10^6$  B16F10 cells s.c. in the flank and treatment with AIPV or subcombination therapies was initiated following the timeline in Fig. 1a. **a**, Tumors were isolated and digested for flow cytometry analysis on day 14. Shown is representative gating for NK cells, polymorphonuclear myeloid cells (PMNs), and monocytic infiltrating cells. **b**, numbers of intratumoral NK cells. **c**, numbers of intratumoral  $CD11b^+ Ly6C^+ Ly6G^-$  monocytic cells **d**, MFI of CD64 on  $CD11b^+ Ly6G^+ Ly6C^{low}$  PMN, taken as a marker for activated anti-tumor neutrophil populations. (shown are boxplots with 5-95% whiskers,  $n = 15$  animals/group, 2 independent experiments). **e-f**, representative haematoxylin and eosin stained sections from untreated (**e**) and AIPV treated (**f**) mice on day 18 after tumor inoculation. ( $n = 5$  animals/group, 3 independent experiments, scale bar = 200  $\mu$ m). **g-h**, Tumors were isolated and analyzed by flow cytometry on day 14 for expression of PD-1 and Tim3. Shown is a representative plot, gated on  $CD8\alpha^+$  T cells (**g**) and fraction of  $PD-1^+ Tim3^+$  of total  $CD8\alpha^+$  T cells quantified by boxplots (whiskers 5-95%) (**h**) ( $n = 15$  animals/group, 2 independent experiments).  $*P < 0.05$ ,  $**P < 0.01$ ,  $***P < 0.001$  by Welch's t test versus untreated with Bonferroni correction.

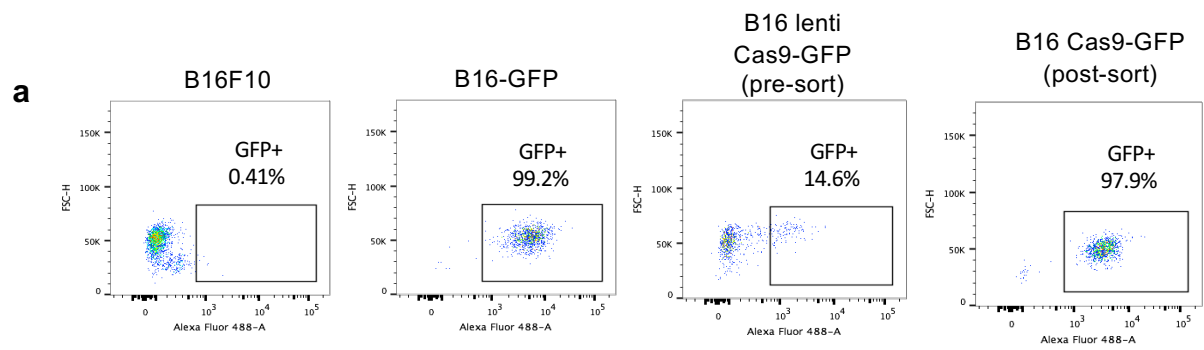
# Supplementary Fig. 7



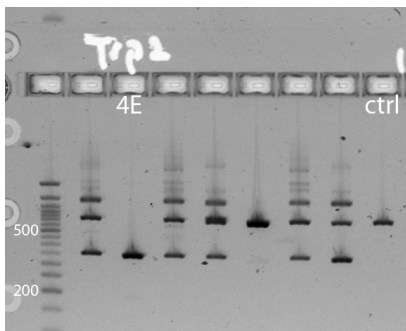
**Supplementary Figure 7: Depletion of selected cellular subsets during AIPV therapy.**

Groups of C57Bl/6 mice ( $n = 10$  animals/group for NK1.1, Ly6G, and CD4 depletion,  $n = 5$ /group for CD8 depletion) were inoculated with  $10^6$  B16F10 cells s.c. in the flank. Cellular subsets were depleted by administering 400  $\mu\text{g}$  of depleting antibody i.p. twice weekly beginning one day prior to initiation of AIPV therapy following the timeline of Fig. 1a. Depletions included CD8<sup>+</sup> T-cells with anti-CD8 $\alpha$ ; CD4 T-cells with anti-CD4; NK cells with anti-NK1.1; neutrophils with anti-Ly-6G; and eosinophils via blockade of IL-5, which was depleted using 1 mg of anti-IL-5 weekly beginning one day prior to treatment. **a**, Confirmation of depletions for CD8<sup>+</sup> T-cells, NK cells, neutrophils, and CD4<sup>+</sup> T-cells from PBMCs on day 14. **b**, Survival of tumor-bearing animals treated with AIPV in the presence of CD4 depletion or IL-5 blockade to eliminate eosinophils. Arrows indicate treatment time points.

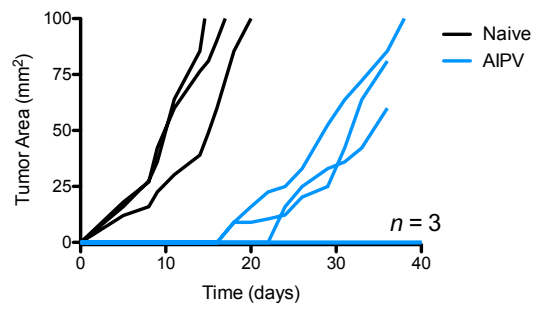
# Supplementary Fig. 8



**b**

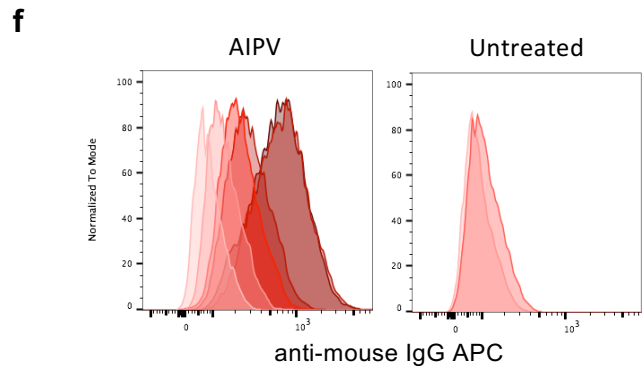
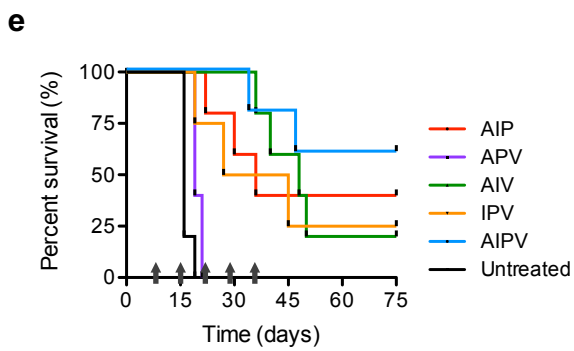
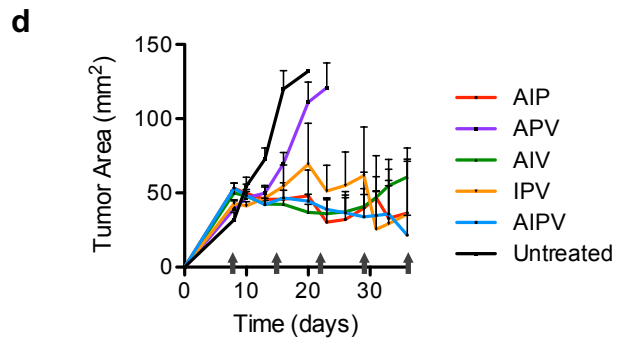
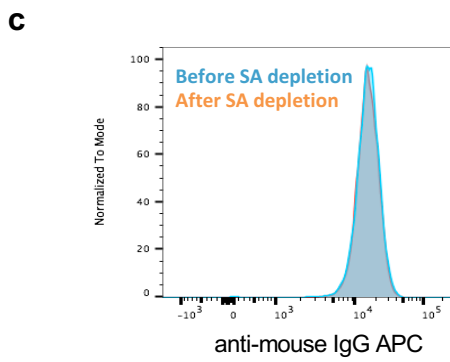
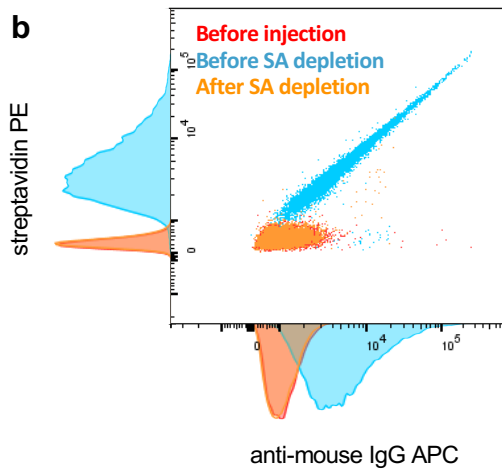
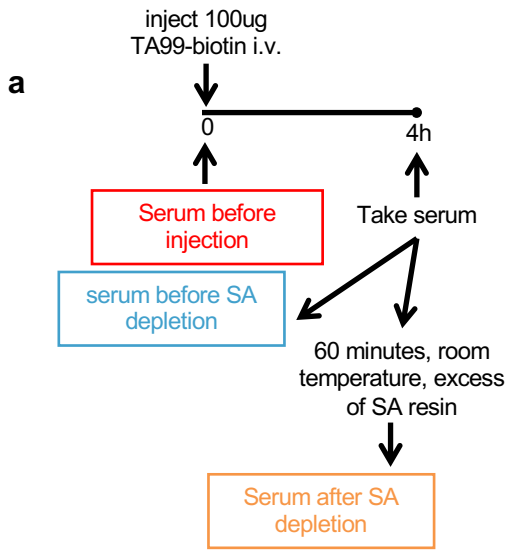


**c**



**Supplementary Figure 8: Generation of a TRP2-KO cell line using Crispr/Cas9.** **a**, B16-GFP-Cas9 cells were generated by transduction of B16F10 cells with lentivirus expressing SpCas9-P2A-EGFP from an EFS promoter. Clones were isolated by single cell flow cytometry for GFP positive cells and evaluated for stable expression. **b**, RNA expression vectors were created by cloning a human U6 promoter and sgRNA sequences into a minimal vector with an ampicillin-selectable marker and a ColE1 replication origin with guide sequences indicated in **Supplementary Table 1**. PCR amplification of an internal region of Trp2 using the sequences shown in **Supplementary Table 2** was performed on clones that grew out of this single cell sort after selection in 2  $\mu\text{g}/\text{mL}$  puromycin. Clone 4E was designated B16-Trp-2KO. **c**, AIPV treated mice that successfully rejected rechallenge with  $10^5$  B16F10 on day 75 were challenged again with  $10^5$  B16-Trp2-KO on day 125. Shown is tumor area over time for individual animals ( $n = 6$  animals/group treated with AIPV and  $n = 3$  age-matched animals/group as naïve controls).

# Supplementary Fig. 9



**Supplementary Figure 9: Depletion of serum TA99 to detect endogenous anti-B16F10 antibody responses during therapy.** **a**, Experimental protocol: Serum was isolated from C57Bl/6 mice immediately prior to and 4 hours following i.v. administration of 100 $\mu$ g of biotinylated TA99. Serum was incubated with an excess of streptavidin agarose for 1h at 25°C and binding to B16F10 was determined using flow cytometry as in Fig. 5a-c. **b**, Shown is one representative of three replicates of dual staining to detect the presence of biotinylated TA99 binding to tumor cells (via streptavidin) and endogenous IgG binding (via anti-mouse IgG secondary), before and after streptavidin agarose depletion of biotin-TA99 from serum. **c**, Serum was isolated from AIPV-treated mice 150 days after rejection of B16F10 and incubated with streptavidin agarose and binding to B16F10 was assessed by flow cytometry. High endogenous IgG binding to B16F10 cells was detected that was not affected by streptavidin agarose depletion. Shown is one representative of three replicates. **d-e**, C57Bl/6 mice were treated with AIPV as indicated in Fig. 1a using biotinylated TA99. Shown are tumor area  $\pm$ s.e.m and survival curves for mice treated with AIPV and subcombinations using biotinylated TA99, showing that use of biotin-TA99 did not interfere with efficacy of the therapy. **f**, C57Bl/6 mice were treated with AIPV as indicated in Fig. 1a using biotinylated TA99. Mice were bled weekly and serum was depleted of TA99-biotin as described above and binding was measured as in Fig 5. Shown is a representative plot of MFI of anti-mouse IgG throughout therapy for an AIPV treated mouse over time ( $n = 5$ /group). Arrows indicate treatment time points.

## Supplementary Tables

### Supplementary Table 1: Guide Sequences

Name	Sequence	Position of Targeted Sequence
Dct-sg 2	5'-CGACTGTAATCGGAAGAAGC GTTTAAGAGCTATGCTGGAAACAGCATAGCAAGTTTAAATAAGGC TAGTCCGTTATCAACTTGAAAAAGTGGCACCGAGTCGGTGC-3'	8991-9013
Dct-sg 4	5'-GAGGCTTGTGACCCGGGTGG GTTTAAGAGCTATGCTGGAAACAGCATAGCAAGTTTAAATAAGGC TGTCCGTTATCAACTTGAAAAAGTGGCACCGAGTCGGTGC-3'	9274-9296

### Supplementary Table 2: Primer Sequences

Name	Sequence	Location
Trp2 forward primer	5'-CACAGAGAACCCTCCGAGAA-3'	8745-8764
Trp2 reverse primer	5'-ACAGGCGGTGTTTGGTAATC-3'	9375-9394